Chemistry SELECT

www.chemistryselect.org

A journal of ChemPubSoc Europe

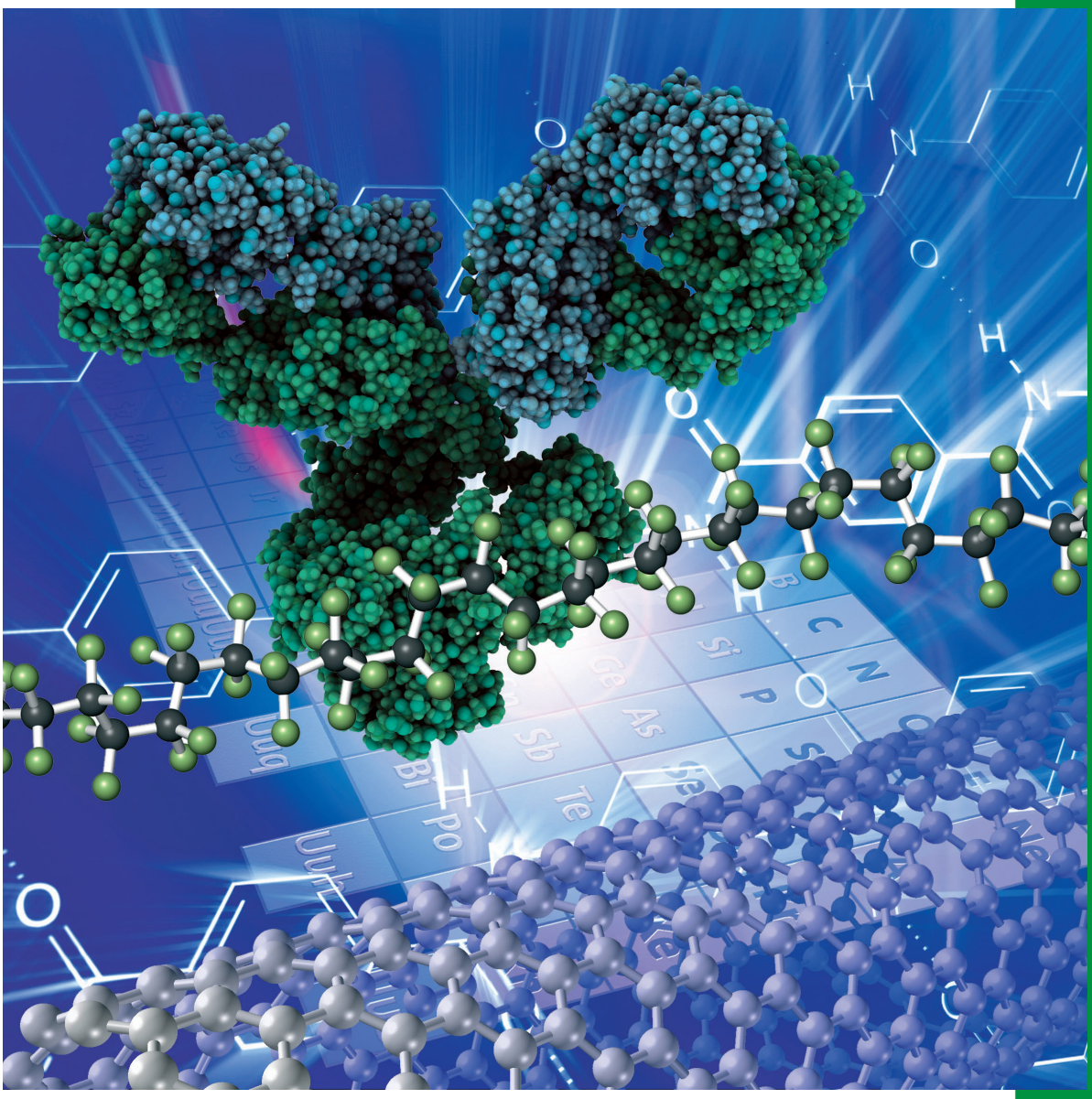

REPRINT

WILEY-VCH

ChemPubSoc Europe

DOI: 10.1002/slct.201701951

Chemistry SELECT Full Papers

Energy Technology & Environmental Science

Nitrogen-Doped Graphene Nanosheets/S Composites as Cathode in Room-Temperature Sodium-Sulfur Batteries

Yong Hao,[a, b] Xifei Li,[c, d] Xueliang Sun,[c] and Chunlei Wang*[a, e, f]

Room-temperature sodium-sulfur (RT Na–S) batteries have gained increasing attention from energy storage community in recent years. In this work, homogeneous nitrogen-doped graphene nanosheets/sulfur (NGNS/S) nanocomposites, synthesized using chemical reaction-deposition method and low temperature heat treatment, were studied as active cathode materials for RT Na–S batteries. Different loading composites with 86%, 65%, 45% and 25% gamma-S_8 have been electrochemically evaluated, respectively, and compared with two control electrodes of NGNS and S. It was found that the NGNS/S composite with 25% S loading exhibited the best electrochemical performance with specific capacities of 212 and 136 mAh g^{-1} in the 1st and 10th cycles, respectively. The enhanced electrochemical performance of NGNS/S nanocomposite is mainly attributed to the improved kinetics due to the NGNS conductive network and easier intercalation of Na^+ into expanded NGNS layers due to the addition of S within the graphene layers. In addition, the composite with 25% S loading shows higher surface area and complete reaction with product of Na_2S, which likely contributes to the improved energy capacity.

Introduction

High energy density and long cycle life batteries are urgently needed to meet the demand in portable electronic devices, electric vehicles and grid-scale stationary storage. Lithium-ion batteries have been widely used in powering portable electronics in the past two decades.[1] However, they are approaching their theoretical energy density limits and facing challenges such as limited resources, safety, cost and efficient energy for large-scale applications. Instead, sodium, with high abundance and suitable redox potential (~2.71 V), could be a cost-effective alternative especially for renewable energy applications where weight and energy density are of minor importance. Sulfur, as another abundant element on earth which has high theoretical capacity of 1675 mAh g^{-1} and high energy density of 2600 Wh kg^{-1}, is becoming one of the most attractive cathode materials to replace traditional transition metal oxide cathodes.[2] It is well known that sodium-sulfur (Na–S) batteries, operating at high temperature conditions (300-350 °C), have been used for stationary energy storage.[3] This high operating temperature could potentially induce severe issues such as corrosion, high power consumption and explosions (In 2012, a Na–S battery fire occurred at Tsukaba Plant in Japan).[3a] In recent years, much effort has been devoted to developing room-temperature (RT) Na–S batteries for mitigating the safety concerns. However, when using traditional Li^+ intercalation electrodes, the large atomic size of Na^+ (1.02 vs 0.59 Å) could cause greater change in the host structure resulting in sluggish diffusion and degradation of cycling performance. Moreover, as analogous to Li–S batteries, RT Na–S batteries undergo some critical issues such as low utilization of sulfur active material, poor cycle life and low storage efficiency. These issues are mainly due to intermediate polysulfides dissolution in electrolytes forming "shuttle" phenomenon, volumetric expansion during cycling and the insulating nature of sulfur.[4]

Although challenges exist in RT Na–S batteries, some work has been reported since 2006.[5] Research efforts have been devoted to developing suitable electrolytes with high ionic conductivity in order to enhance the cell performance.[5a,f] Solid PEO polymer electrolyte and PVDF gel polymer electrolyte have been studied, and relatively high sodium ion conductivity (~10^{-4} S cm^{-1}) has been achieved.[5c,d] Further, liquid electrolytes such as ether-based electrolyte or other solvents (e.g. EC, DMC, PC) with sodium salt such as $NaCF_3SO_3$ or $NaClO_4$ have been used to promote the formation of the intermediate products polysulfides during the charge and discharge processes.[5e,g] However, the well-known shuttle effect of polysulfides in the electrolyte has become the major issue. Recently, more efforts

[a] Dr. Y. Hao, Prof. C. Wang
Department of Mechanical and Materials Engineering, Florida International University, 10555 W. Flagler St., Miami, FL 33174, USA
E-mail: wangc@fiu.edu
[b] Dr. Y. Hao
Materials Engineering Department, California Polytechnic State University, 1 Grand Avenue, San Luis Obispo, CA 93407, USA
[c] Prof. X. Li, Prof. X. Sun
Nanomaterials and Energy Lab, Department of Mechanical and Materials Engineering, Western University, London, Ontario N6 A 5B9, Canada
[d] Prof. X. Li
Institute of Advanced Clean Energy, Xi'an University of Technology, Xi'an 710048, China
[e] Prof. C. Wang
Advanced Materials Engineering Research Institute, Florida International University, 10555 W. Flagler St., Miami, FL 33174, USA
[f] Prof. C. Wang
Center for the Study of Matter at Extreme Conditions, Florida International University, University Park, Miami, FL 33199, USA

Supporting information for this article is available on the WWW under https://doi.org/10.1002/slct.201701951

have been focused on developing advanced electrode materials and novel cell configurations to prohibit the polysulfides diffusion to Na electrode, such as applying an ion selective Nafion-coating membrane as a separator,[5h] inserting a carbon-based interlayer between cathode and separator,[5i,j] and using Na–S reduction products (e.g. sodium polysulfide catholytes or Na_2S) as cathode materials.[5k,l] Xin *et al.* employed carbon materials as a matrix to improve the utilization of S and confine the polysulfides.[5m] Yu *et al.* applied carbon materials, Nafion-coating separator and polysulfide catholytes to enhance the capacity retention.[5n,o] So far as it concerns, the effective carbon materials conducted in RT Na–S batteries have been involved with carbon nanofiber, mesoporous carbon, microporous carbon and hard carbon.[5p,q] Besides, Hwang *et al.* concluded that the electrochemical performance of RT Na–S batteries is dependent on the sulfur content, for instance, in the S/carbon nanofiber composite, S loading below 48% is beneficial for a good performance.[5p]

Graphene, with a unique two-dimensional (2D) carbon structure, has been widely used in Li-ion batteries since its discovery due to its exceptional electrical conductivity, high specific surface area, and high mechanical strength.[6] In our previous work, we have reported a promising N-doped graphene nanosheets/sulfur (NGNS/S) composite as cathode in lithium-sulfur batteries.[7] N-doping can easily modify local electronic structures of graphene and enhance binding of other ions with the 2D layers.[7–8] Graphene with N-functional groups has been used as a conductive framework to facilitate immobilization of sulfur discharge products in several Li–S works. For instance, Mathiram et al. proved that N functional groups can effectively improve the affinity and binding energy between the N heteroatoms and lithium polysulfides/Li_2S and significantly enhance the electrochemical performance of Li–S batteries.[9] Zhang et al. used computational approach to demonstrate that the binding energies for N-doped graphene with atomic Li and Li polysulfides are stronger compared to the case of primitive graphene, which proposed that the electrochemical enhancement could be attributed to strong ionic attractions between N heteroatoms and Li cations instead of S anions.[10] Lou et al. reported exceptional performance in Li–S batteries due to amino-functionalized reduced graphene oxide covalently stabilized S and lithium polysulfides on its surface with good conductivity and high mechanical stability.[11] However, in terms of RT Na–S battery, according to our knowledge, no research has been published to utilize N-doped graphene or its composite as electrode component. It is of our interest to study the possibility of minimizing shuttle effect of the sodium polysulfides using N functional groups and verify the feasibility of 2D N-doped graphene in RT Na–S battery application. In this contribution, NGNS/S nanocomposites with various weight loadings of S were fabricated and evaluated as cathode in RT Na–S batteries. A thermal treatment for the NGNS/S composite was conducted with the aim of better encapsulating S into the graphene layers and improving the kinetics. The electrochemical testing results show that NGNS/S composite with 25% S loading exhibits a better performance in terms of capacity retention, cycle life and rate capability in comparison with other loading composites. It has been found that S loading in the composite is one of the crucial factors on its electrochemical performance.

Results and discussion

NGNS/S nanocomposite was synthesized by a facile chemical reaction-deposition method,[12] and followed by low temperature heat treatment, as shown in Figure 1. Thermogravimetric analysis (TGA) was carried out to confirm the weight percentages of S in the NGNS/S composites. As shown in Figure S1a, the weight loss of as-prepared high S loading sample before heat treatment is ~90 wt. %, referred as NGNS/S-90. After heat treatment at 155°C, S loading content was reduced to ~86 wt. %, referred as NGNS/S–H86 in the following content. In Figure S1b, it can be observed that the NGNSH has a weight loss of ~5 wt. % after heat treatment, which is mainly due to the moisture evaporation. The NGNS/S-30 sample has been obtained with ~30 wt. % of sulfur before heat treatment and ~25 wt. % of sulfur remaining after heat treatment, which is referred as NGNS/S–H25 in the following. In Figure S1c and S1d, the initial sulfur loading of ~69 wt. % and ~48 wt. % for NGNS/S-69 and NGNS/S-48, respectively, reduced to ~65 wt. % and ~45 wt. % for NGNS/S–H65 and NGNS/S–H45 after heat treatment, respectively. Figures S2a and S2b show the N_2 adsorption-desorption isotherms of NGNS/S–H86, sulfur, NGNSH and NGNS/S–H25, respectively. Brunauer-Emmett-Teller (BET) results derived from Figure S2a and S2b show that NGNSH, NGNS/S–H25, NGNS/S–H86, and S exhibit the surface area of 570, 272, 6.5, and 1.2 $m^2\ g^{-1}$, respectively. It indicates that the surface area of nanocomposite decreases with the increase of S loading.

The X-ray diffraction (XRD) patterns of S, NGNS/S–H86, NGNS/S–H65, NGNS/S–H45, NGNS/S–H25, NGNSH, and graphene nanosheets (GNS) are presented in Figure 2. A broad diffraction peak at around 24° can be observed in the GNS curve, corresponding to the characteristic (002) plane of multi-layered graphene. The XRD pattern of NGNSH shows the peak position of (002) plane shifts to around 26°. This small change of peak position indicates that the nitrogen defect sites were successfully doped into the NGNS during the ammonia corrosion treatment process, which is in good agreement with other reports.[13] The XRD pattern of the heat-treated sulfur generally exhibits a series of sharp and strong peaks, indicating a well-defined Fddd orthorhombic crystalline structure of alpha-S_8 (JCPDS#: 00–008-0247). A series of sharp peaks can be observed on the XRD pattern of NGNSs/S–H86 nanocomposite indicating that sulfur particles in NGNSs/S–H86 nanocomposite are in the form of gamma-S_8 with P2/c monoclinic crystalline structure (JCPDS#: 01–071-0396). In the XRD pattern of NGNS/S–H65, a major peak can be observed at 26° which is assigned to (002) plane of NGNS. The other peaks match the P2/c monoclinic structure of S, indicating S as gamma-S_8 exists in NGNS/S–H65. The peaks of multi-layered graphene and gamma-S_8 can also be observed on both XRD patterns of NGNS/S–H45 and NGNS/S–H25. The XRD investigation reveals that the phase change of S from alpha-Sulfur8 to gamma-S_8 in

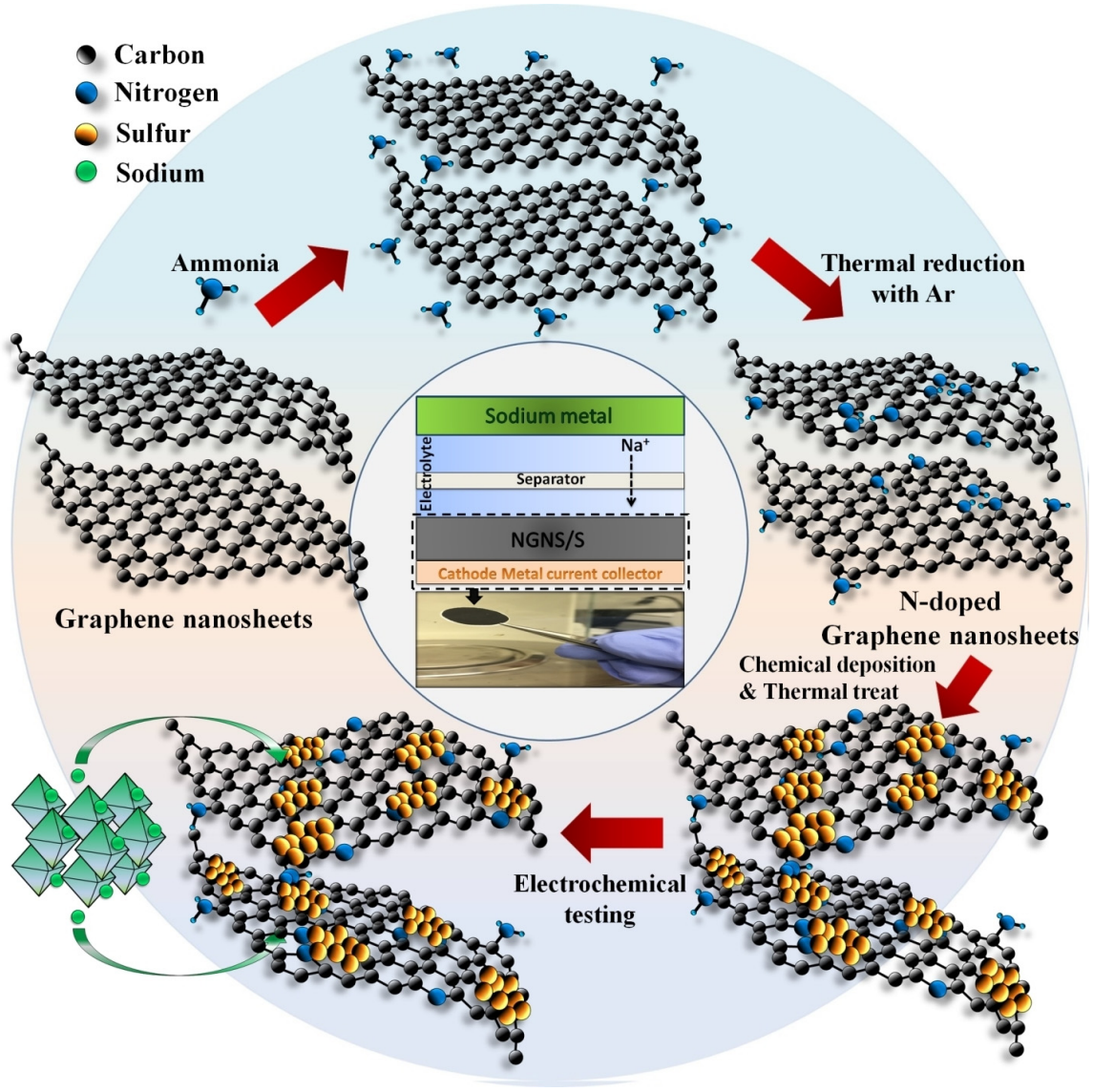

Figure 1. Schematic illustration of Nitrogen-doped Graphene nanosheets/Sulfur nanocomposites preparation and electrochemical testing as cathode material in room-temperature Sodium-Sulfur batteries; typical room-temperature sodium-sulfur batteries configuration with actual working electrode picture (middle).

all of the composite samples could be due to thermal effect and/or nano-confinement of melted S diffused into NGNS.

The scanning electron microscope (SEM) and Transmission Electron Microscope (TEM) images of NGNSH, NGNS/S–H25 and NGNS/S–H86 nanocomposites are shown in Figures 3 and S3, respectively. Figure 3a displays that the sizes of randomly distributed NSNSH particles vary in micron scale. From Figure 3a inset, it can be clearly observed that numerous NGNSH layers are stacked together. The TEM image (Figure 3b) of ultrasound dispersed NGNSH substrates shows a wrinkled two-dimensional layered structure. From Figures 3c and S3, it can be seen that both NGNS/S–H25 and NGNS/S–H86 nanocomposites show a 3D hierarchical voile-like structure with less agglomeration. EDS mappings show uniform distribution of S in both NGNS/S–H25 and NGNS/S–H86 nanocomposites (not shown). High-resolution TEM was conducted on the ultrasonic dispersed NGNS/S–H25 nanocomposite, as shown in Figure 3d. Irregularly shaped single crystalline S particles ranging from 7 ~ 15 nm can be observed. The measured lattice fringe with an interplanar distance of 3.30 Å can be assigned to the (022) plane of monoclinic gamma-S_8.

Electrochemical evaluation of NGNS/S–H25, NGNS/S–H45, NGNS/S–H65 and NGNS/S–H86 nanocomposites along with two control samples of S and NGNSH was conducted at room temperature. Let's first take a look at the case of S loading less than 50%. From the cyclic voltammetry (CV) profiles of NGNS/S–H25 in Figure 4a, it can be observed that there is a sharp cathodic peak at potential of 2.18 V during the reduction process in the 1st cycle. This peak could be attributed to the formation of long chain polysulfides Na_2S_n ($4 \leq n \leq 8$).[5i] Another small broad cathodic peak at ~1.5 V with the following sweeping until the cut-off voltage corresponds to the reduction

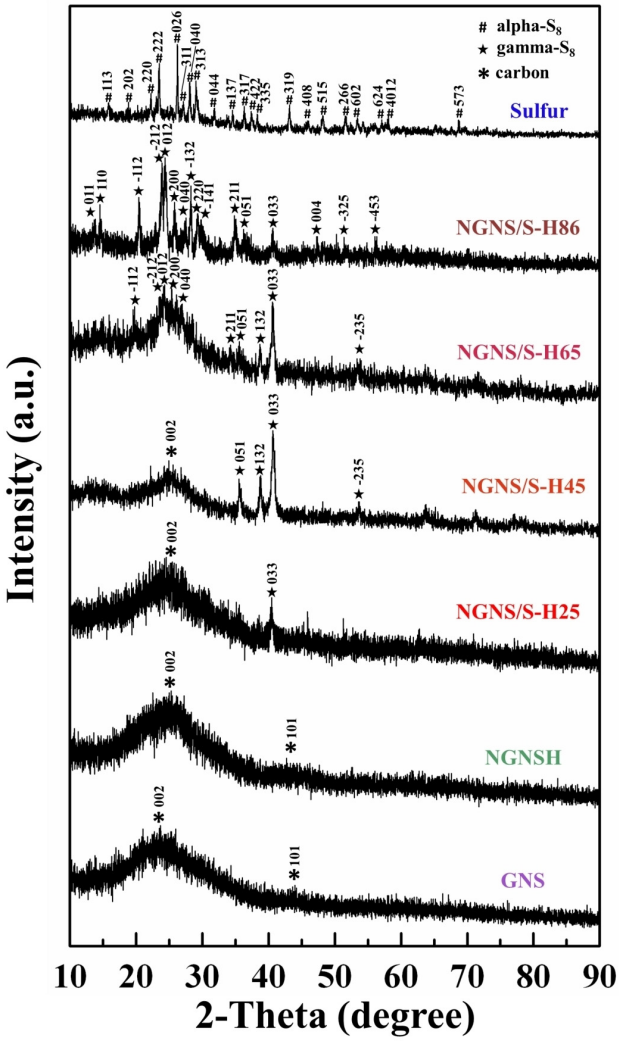

Figure 2. XRD patterns of Sulfur, GNS, NGNSH, NGNS/S–H25, NGNS/S–H45, NGNS/S–H65 and NGNS/S–H86 nanocomposites, respectively.

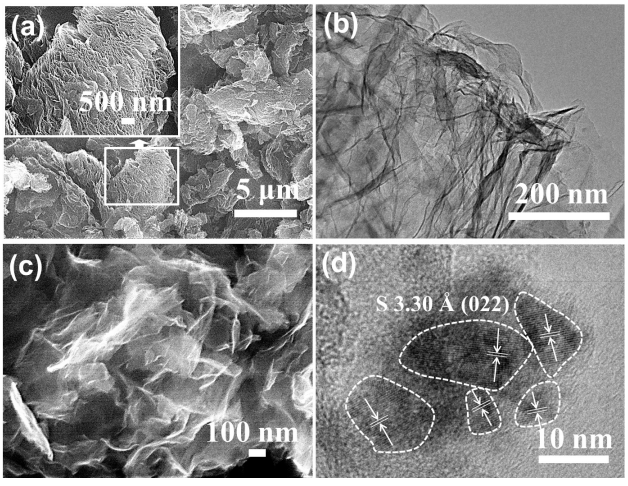

Figure 3. (a) SEM image of NGNSH, inset represents a typical layered structure of NGNSH, (b) TEM image of NGNSH, (c) SEM image of NGNS/S–H25, and (d) HRTEM image of NGNS/S–H25.

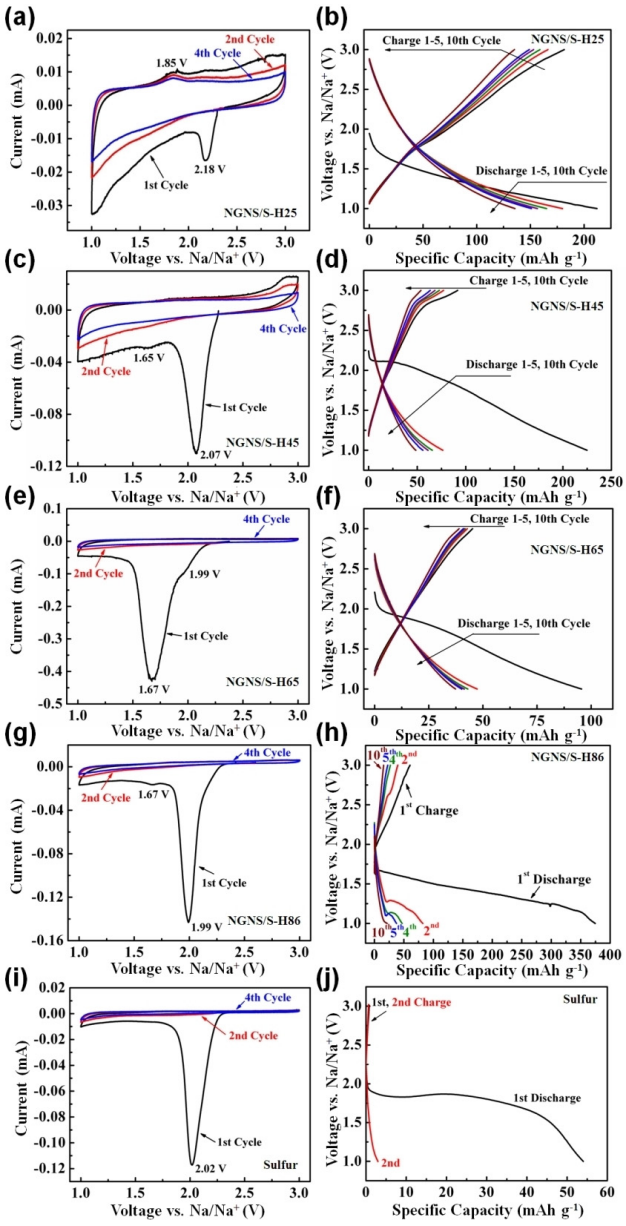

Figure 4. CV curves of (a) NGNS/S–H25, (c) NGNS/S–H45, (e) NGNS/S–H65, (g) NGNS/S–H86 and (i) sulfur, respectively, at a scan rate of 0.1 mV s^{-1} between 1.0 and 3.0 V vs. Na/Na^+; Galvanostatic discharge/charge profiles of (b) NGNS/S–H25, (d) NGNS/S–H45, (f) NGNS/S–H65, (h) NGNS/S–H86 and (j) sulfur, respectively.

process of long chain polysulfides to Na_2S.[14] In the reverse oxidation process in the 1st cycle, there is an anodic peak centered at 1.85 V, indicating that Na_2S has been oxidized to short chain polysulfides Na_2S_n ($2 \leq n < 4$) and Na_2S_4.[5i] Another small anodic peak observed at ~2.23 V is assigned to the oxidation process of Na_2S_4 to Na_2S_8 and S.[5j] After the current sweeps back to the reduction process of 2nd cycle, the long chain polysulfides related cathodic peak can barely be observed. This disappearance of cathodic peak may be due to the soluble polysulfides Na_2S_n ($4 \leq n \leq 8$) dissolve and dissipate in the electrolyte during the first cycle or the precipitation of

insoluble Na_2S_n ($1 \leq n < 4$) as solid phases which may have a detrimental effect on the kinetics of Na-ion diffusion into the electrode.[15] From the oxidation curves of the 2nd to 4th cycles, the anodic peaks can be observed with less intensity change. Figure 4b exhibits the charge/discharge profiles of NGNS/S–H25 at 0.05C. There is no obvious plateau observed from the discharge curves. Wang *et al.* reported similar discharge behavior of S/polymer composite in RT Na–S batteries.[5b] From the charge curves, an oxidation plateau shown at 1.85 V can be observed, which is consistent with the CV performance. The discharge/charge capacities have been reached 212 mAh g^{-1} and 181 mAh g^{-1} in the 1st cycle, respectively. The rate capability of NGNS/S–H25 from 0.05C to 5C is shown in Figure 5a. At each rate, the discharge capacities at the 10th

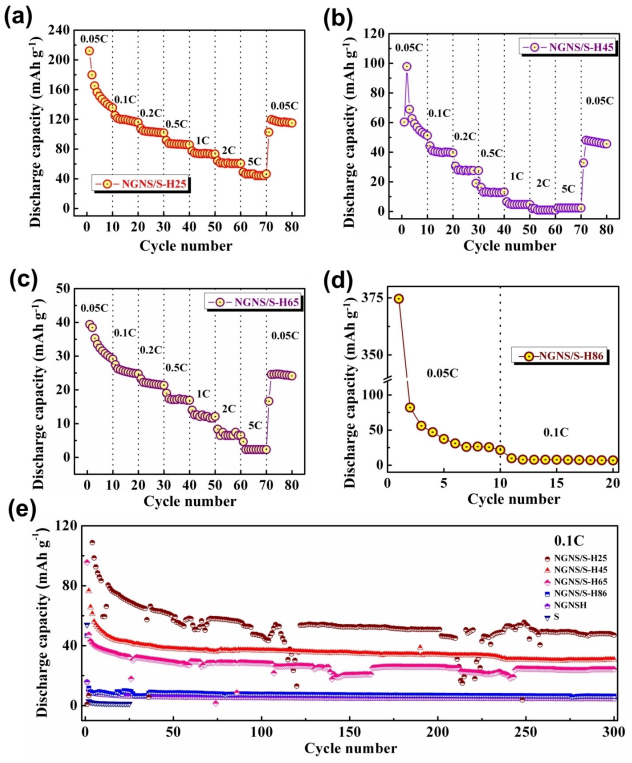

Figure 5. Rate performances of (a) NGNS/S–H25, (b) NGNS/S–H45 and (c) NGNS/S–H65 at various C rates and (d) NGNS/S–H86 at 0.05C and 0.1C; (e) Cycling performances of NGNS/S–H25, NGNS/S–H45, NGNS/S–H65, NGNS/S–H86, NGNSH and S electrodes at 0.1C, respectively.

cycle are 136, 116, 102, 86, 73, 61 and 46 mAh g^{-1} at rates of 0.05C, 0.1C, 0.2C, 0.5C, 1C, 2C and 5C, respectively. During the 1st cycle of 0.2 C, the discharge and charge capacities are 108 mAh g^{-1} and 105 mAh g^{-1}, respectively, which exhibit better capacity values compared to the reported work of N-doped carbon coating $Na_3V_2(PO_4)_3$ electrode at 0.2 C.[16] When the rate comes back to 0.05C after high rates, the specific capacity is about 115 mAh g^{-1} at the 80th cycle. Figure 4c shows the CV profile of NGNS/S–H45, similar to NGNS/S–H25, a sharp cathodic peak shows at 2.07 V in the 1st cycle, representing the long chain polysulfides Na_2S_n ($4 \leq n \leq 8$) formation. A small cathodic peak at 1.65 V attributing to the formation of Na_2S can be observed with following reduction process. During the oxidation process, a broad anodic peak at ~ 1.85 V and a small peak at ~2.85 V can be observed, indicating the Oxidation of Na_2S to short chain polysulfides and further to long chain polysulfides and S. From the following reduction process of 2nd and 4th cycles, there are barely cathodic peaks observed. The anodic peaks can be observed at the same position during the oxidation process of the following cycles. Figure 4d shows the charge/discharge curves of NGNS/S–H45. During the discharge of 1st cycle, there is a plateau observed at ~2.1 V, corresponding to S transforming to long chain polysulfides Na_2S_n ($4 \leq n \leq 8$), which matches the CV performance. The charge curve of 1st cycle exhibits a plateau at 2.85 V, which also matches the CV curve. There are no clear plateaus on the following discharge curves and the charge curves exhibit same plateau at 2.85 V as the 1st discharge curve. The rate performance of NGNS/S–H45 is shown in Figure 5b, exhibiting capacity recovery after the current rate return back to 0.05C. Electrochemical performance of control sample NGNSH electrodes are shown in Figure S6. From the rate capability of NGNSH in Figure S6c, it shows that the discharge capacities only reach 9, 6, 5, 3, 0.5, 0.5, 0.6 and 7 mAh g^{-1} at the 10th cycle of 0.05C, 0.1C, 0.2C, 0.5C, 1C, 2C 5C and 0.05C, respectively. The NGNS/S–H25 and NGNS/S–H45 electrodes present better rate capability as compared to pure NGNSH. According to the CV and charge-discharge results above, the discharge process of NGNS/S–H25 and NGNS/S–H45 involve the transition of sulfur to dissolved Na_2S_8 and Na_2S_4. Na_2S_4 is further reduced to Na_2S_2 and Na_2S. It is in good agreement with the work that Manthiram *et al.* reported where the similar electrochemical reactions can be presented as following:[5j,14a]

$$S_8 + 2Na^+ + 2e^- \rightarrow Na_2S_8 \ (\sim 2.20\,V) \quad (1)$$

$$Na_2S_8 + 2Na^+ + 2e^- \rightarrow 2Na_2S_4 \ (2.20 - 1.65\,V) \quad (2)$$

$$Na_2S_4 + 2Na^+ + 2e^- \rightarrow 2Na_2S_2 \ (\sim 1.65\,V) \quad (3)$$

$$Na_2S_2 + 2Na^+ + 2e^- \rightarrow 2Na_2S \ (1.65 - 1.20\,V) \quad (4)$$

Next, let's look into the electrochemical performance for the S loading more than 50%. The CV curves of NGNS/S–H65 are shown in Figure 4e. There is one small reduction peak at 1.99 V and followed by a strong peak at 1.67 V during the cathodic process of the first cycle. The first peak represents the reduction process of S to Na_2S_4 and Na_2S_2 and the second peak represents further reduction of Na_2S_4 and Na_2S_2 to Na_2S. There are no oxidation peak and reduction peaks in the following 2nd and 4th cycles observed. The charge/discharge curves of NGNS/S–H65 are presented in Figure 4f. There is one major plateau at 1.99 V during the discharge process of the 1st cycle, indicating the formation of Na_2S_4 and Na_2S_2. There are no plateaus on charge/discharge curves in the following cycles, which is in consistence with the CV curves. The NGNS/S–H65 electrode exhibited worse rate capability than low loading nanocomposite NGNS/S–H25, as shown in Figure 5c. The

electrochemical performances of NGNS/S–H86 are presented in Figures 4g and 4 h. From the CV profile of NGNS/S–H86 as shown in Figure 4g, there is one strong reduction peak observed at 1.99 V during the cathodic process of the 1st cycle. This reduction peak could be assigned to the reduction reaction of S to Na_2S_4 and Na_2S_2.[5f] A small reduction peak is observed at 1.67 V, which is attributed to Na_2S_2 transferring to sulfide Na_2S.[5f] During the anodic process of the 1st cycle, there are no obvious oxidation peaks shown up in the curve. From the following cathodic and anodic sweep in the 2nd and 4th cycles, there are no obvious reduction and oxidation peaks observed on the CV curves of NGNS/S–H86. This phenomenon might be due to the formation of irreversible sodium polysulfides which could not recover to sulfur during charge process or the dissolution of sodium polysulfides into the electrolyte.[5a] The galvanostatic charge/discharge profile of NGNS/S–H86 cathode is shown in Figure 4h. A typical plateau at 1.7 V is observed on the discharge curve of 1st cycle, which can be assigned to the formation of sodium sulfide Na_2S.[5f,14b] A relatively high discharge capacity of 375 mAh g^{-1} is obtained at a cutting voltage of 1.0 V. During the second cycle, there are plateaus observed on both charge and discharge curves at 2.63 V and 1.25 V, respectively. The discharge capacity reduces to 82 mAh g^{-1} at the 2nd cycle, and at the 10th cycle only limited capacity ~25 mAh g^{-1} still remains. There are small plateaus observed on the discharge curves of the following 4th, 5th and 10th cycles, which reveal that S is constantly reduced to polysulfides in each cycle. However, the voltages of the plateaus show lower and lower with capacity reduction during cycling. This voltage drop might be attributed to the formation of surface film and the ion transfer across the liquid/solid interface.[5f] From rate performance of NGNS/S–H86 in Figure 5d, it can be observed that the capacity at 0.05C of NGNS/S–H86 reduced from 375 mAh g^{-1} of the 1st cycle to ~25 mAh g^{-1} of the 10th cycle. At 0.1C, only ~5 mAh g^{-1} remains. The CV and charge/discharge results of pure sulfur are shown in Figure 4i and 4j. In Figure 4i, There is one strong reduction peak observed at 2.02 V in the cathodic process of 1st cycle, representing S reduce to the polysulfides Na_2S_4 and Na_2S_2.[5f] In Figure 4j, the discharge capacity from 55 mAh g^{-1} in the 1st cycle dramatically decreases to 3 mAh g^{-1} in the 2nd cycle. The failure of pure S electrode could be due to the dissolution of polysulfide and irreversible precipitation formation. From the electrochemical performance of NGNS/S–H65 and NGNS/S–H86, it reveals that the conductive matrix could not efficiently prevent the dissolution of polysulfide, leading to the poor rate capability and poor reversibility with the increasing of cycle numbers. The CV results for high S loading samples also suggest that Na_2S_4 and Na_2S_2 are mainly involved during the reduction of sulfur, which were in good agreement with Janek *et al.*'s work.[5f,15] From the CV curves of low loading (< 50% S) and high loading (>50% S) nanocomposites, the irreversible CV behaviors show that the dissolution of polysulfides leads to the incomplete redox reaction between Na and S after initial cycles. The absence of plateaus from the charge-discharge curves indicates the majority contribution of capacity coming from the sloping region reaction, i.e. $Na_2S_8 + 2Na^+ + 2e^- \rightarrow 2Na_2S_4$. In future, more detailed work need to be carried out to confirm the cell electrochemistry of RT Na–S batteries and how it affects the cell performance.

Cycling performance has been carried out on NGNSH, S, NGNS/S–H86, NGNS/S–H65, NGNS/S–H45 and NGNS/S–H25 electrodes, respectively, as shown in Figure 5e. The unavoidable power outrage in south Florida has also been recorded in the cycling test result. It can be observed that the NGNS/S–H25 electrode exhibits a better cycling performance upon 300 cycles at 0.1 C showing about 48 mAh g^{-1} retaining at the 300th cycle. It has to be noted that the specific capacity in this work has been calculated based on the mass of sulfur in the electrodes before cycling without considering the S loss during the cycling. The performance of NGNS/S composites is much better as compared to the control sample pure S, indicating that NGNS with N-functional groups are not just the contributor of improving conductivity, but have positive effect on the immobilization of S and its discharge products. However, the capacity drop with cycling indicates that the confinement effect of NGNS to S and polysulfides was still not excellent enough in the RT Na–S batteries owing to inherent structural nature of graphene as well as limited N content in NGNS. The S consumption as polysulfides which dissolved into the electrolyte could be the main reason which led to the capacity loss during cycling test. We believe by optimizing the structure and N content of NGNS, the confinement effect of S and polysulfides will be enhanced. This investigation will be conducted as our future work.

To examine the charge transfer resistance and Na^+ diffusion kinetics, electrochemical impedance spectroscopy (EIS) of the NGNS/S–H25 NGNS/S–H45, NGNS/S–H65 and NGNS/S–H86 cells has been conducted before the 1st cycle and after the 300th cycle. As the Nyquist plots shown in Figures 6a–6d, it can

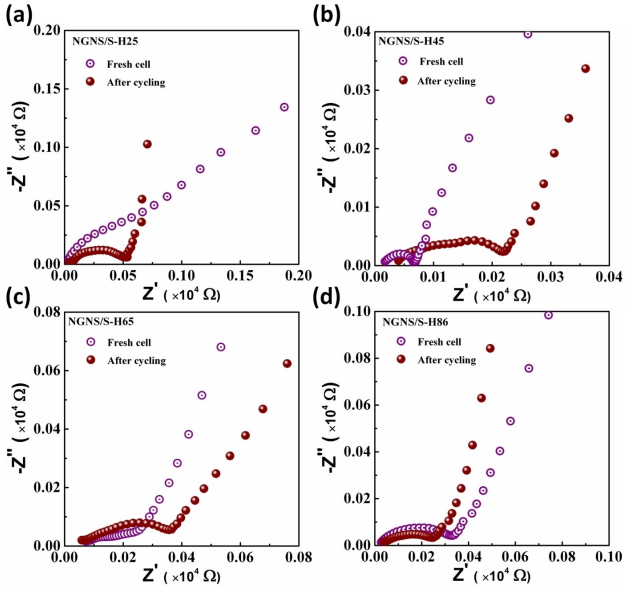

Figure 6. Nyquist plots of (a) NGNS/S–H25, (b) NGNS/S–H45, (c) NGNS/S–H65 and (d) NGNS/S–H86 working electrodes before 1st and after 300th cycles, respectively.

be observed that both semicircles in the high frequency range of NGNS/S–H25 and NGNS/S–H86 after cycling are smaller than fresh cells, which indicates a better charge-transfer condition after cycling. The semicircles in the high frequency range of NGNS/S–H45 and NGNS/S–H65 after cycling are little bigger than the fresh cell, indicating the charge transfer resistance becoming higher than before cycling The coin cell of NGNS/S–H25 was fully charged to 3.0 V after cycling and disassembled inside the glove box. SEM and TEM investigations were conducted after the electrode was rinsed with DMC, and dried under vacuum at room temperature, as shown in Figure 7a and

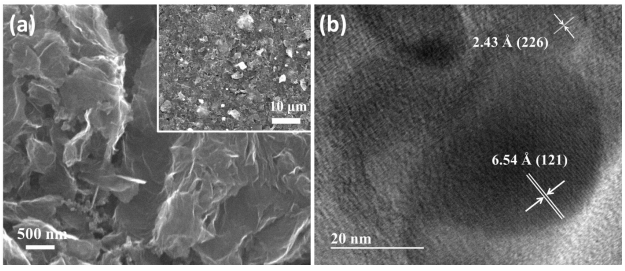

Figure 7. (a) SEM image of NGNS/S–H25 electrode after 300th cycles (inset is in low resolution). (b) TEM image of Na_2S in NGNS/S–H25 electrode after 300th cycles (in fully charged condition).

7b. From the TEM image of dispersed NGNS/S–H25 electrode, the measured distances of interplanar fringes are 6.54 Å and 2.43 Å which are assigned to the (121) and (226) planes of Na_2S. This verifies that the final reduction product of S and Na is Na_2S. This Na_2S may be coming from the precipitation on the surface of NGNS/S composites and could not be completely oxidized to S even at a fully charged state, indicating that irreversible redox reaction could also contribute the capacity drop during cycling. Compared to other work of RT Na–S batteries,[5a,d–f] our N-doped graphene and S composites still have issues related to S dissolution. In this work, it is the first time to investigate N-doped graphene as a conductive matrix to immobilize sulfur and polysulfides in the RT Na–S batteries. We have synthesized the NGNS/S composites with different loadings, i.e. 25 wt. %, 45 wt. %, 65 wt. % and 86 wt. %. It shows that the electrochemical performance at low loading 25 wt. % is favorable to the performance which is lower than the value reported in Ref. 5p but with a similar trend. Although the practical use of the composite electrode is undermined with lower loading, the 25 wt. % NGNS/S composites exhibit much better electrochemical performance as compared to control sample pure S, indicating that the strategy of using NGNS/S composites at low loading has a positive effect on the RT Na–S batteries performance. The electrochemical improvement could be attributed to the conductive network established by both S and NGNS, relatively low S loading, and stronger binding effect from N-doped graphene with mitigated shuttle effect. Although there are partial dissolution of polysulfides during cycling and low loading composites exhibit the best electrochemical performance among other loadings, it is worthy to be noted that the performance of NGNS is also involved with several factors, such as the type of N functional groups, the N content in the NGNS, and structural property of NGNS induced by N-doping, etc. Based on our work, further improvement with high loading of S can be expected by optimizing the concentration of N functional groups as well as creating nanopores of N-doped graphene. In future work, more efforts need to be done to improve the S loading in the composite materials and to understand how loading and different types and different quantity of functional groups affect the performance improvement.

Conclusions

In summary, we have demonstrated NGNS/S nanocomposites with different sulfur loading as electrode materials for RT Na–S batteries, respectively. In these nanocomposites, sulfur has been phase-transferred from alpha-S_8 to gamma-S_8 during the thermal treatment progress. The NGNS/S–H25 nanocomposite exhibits a better electrochemical performance in terms of rate capability and cyclability as compared to other higher loading NGNS/S nanocomposites. This electrochemical improvement can be attributed to the conductive network established by both S and NGNS for enhanced Na^+ transport. NGNS as confinement host played a relatively effective role in immobilizing low loading of sulfur and confining polysulfides during cycling. To achieve the high loading of sulfur with best electrochemical performance, optimizing the structural property and N concentration of NGNS will be further investigated in the future study.

Supporting Information Summary

Experimental Section, Figure S1, Figure S2, Figure S3, Figure S4 and Figure S5 are included in this part. Figure S1 is TGA analysis of (a) NGNS/S–H86 and NGNS/S-90, (b) NGNSH, NGNS/S–H25 and NGNS/S-30, (c) NGNS/S–H65 and NGNS/S-69, and (d) NGNS/S–H45 and NGNS/S-48. Figure S2 is BET results of (a) NGNS/S–H86 and Sulfur, and (b) NGNSH and NGNS/S–H25. Figure S3 is SEM image of NGNS/S–H86. Figure S4 is (a) XPS spectrum and (b) N2 adsorption-desorption isotherms of GNS. Figure S5 is electrochemical performance of NGNSH electrodes in RT Na–S cells: (a) cyclic voltammograms (b) discharge/charge profile and (c) rate capability.

Acknowledgments

This work is partially supported by the NSF projects (No. 1506640 and No. 1509735) and NSF NERC ASSIST center seed funding. Y. Hao acknowledges Doctoral Evidence Acquisition (DEA) Fellowship from UGS at FIU and facilities of AMERI at FIU. C. Wang acknowledges Changbaishan Scholarship from Jilin University.

Conflict of Interest

The authors declare no conflict of interest.

Keywords: cathode · N-doped graphene · nanocomposites · room-temperature Na–S batteries · sulfur

[1] a) J. M. Tarascon, M. Armand, *Nature* **2001**, *414*, 359–367; b) A. S. Arico, P. Bruce, B. Scrosati, J. M. Tarascon, W. Van Schalkwijk, *Nat. Mater.* **2005**, *4*, 366–377; c) X. Li, A. Dhanabalan, L. Gu, C. Wang, *Adv. Energy Mater.* **2012**, *2*, 238–244.

[2] P. G. Bruce, S. A. Freunberger, L. J. Hardwick, J. M. Tarascon, *Nat. Mater.* **2012**, *11*, 19–29.

[3] a) B. L. Ellis, L. F. Nazar, *Curr. Opin. Solid State Mater. Sci.* **2012**, *16*, 168–177; b) T. Oshima, M. Kajita, A. Okuno, *Int. J. Appl. Ceram. Technol.* **2004**, *1*, 269–276; c) Z. Wen, Y. Hu, X. Wu, J. Han, Z. Gu, *Adv. Funct. Mater.* **2013**, *23*, 1005–1018.

[4] a) X. Ji, K. T. Lee, L. F. Nazar, *Nat. Mater.* **2009**, *8*, 500–506; b) X. Ji, S. Evers, R. Black, L. F. Nazar, *Nat. Commun.* **2011**, *2*, 325; c) S. Evers, T. Yim, L. F. Nazar, *J. Phys. Chem. C* **2012**, *116*, 19653–19658.

[5] a) C. W. Park, J. H. Ahn, H. S. Ryu, K. W. Kim, H. J. Ahn, *Electrochem. Solid-State Lett.* **2006**, *9*, A123-A125; b) J. Wang, J. Yang, Y. Nuli, R. Holze, *Electrochem. Commun.* **2007**, *9*, 31–34; c) C. W. Park, H. S. Ryu, K. W. Kim, J. H. Ahn, J. Y. Lee, H. J. Ahn, *J. Power Sources* **2007**, *165*, 450–454; d) J. S. Kim, H. J. Ahn, I. P. Kim, K. W. Kim, J. H. Ahn, C. W. Park, H. S. Ryu, *J. Solid State Electrochem.* **2008**, *12*, 861–865; e) H. Ryu, T. Kim, K. Kim, J. H. Ahn, T. Nam, G. Wang, H. J. Ahn, *J. Power Sources* **2011**, *196*, 5186–5190; f) S. Wenzel, H. Metelmann, C. Raiß, A. K. Dürr, J. Janek, P. Adelhelm, *J. Power Sources* **2013**, *243*, 758–765; g) D. J. Lee, J. W. Park, I. Hasa, Y. K. Sun, B. Scrosati, J. Hassoun, *J. Mater. Chem. A* **2013**, *1*, 5256–5261; h) I. Bauer, M. Kohl, H. Althues, S. Kaskel, *Chem. Commun.* **2014**, *50*, 3208–3210; i) X. Yu, A. Manthiram, *J. Phys. Chem. Lett.* **2014**, *5*, 1943–1947; j) X. Yu, A. Manthiram, *ChemElectroChem* **2014**, *1*, 1275–1280; k) X. Yu, A. Manthiram, *J. Phys. Chem. C* **2014**, *118*, 22952–22959; l) X. Yu, A. Manthiram, *Chem. - Eur. J.* **2015**, *21*, 4233–4237; m) S. Xin, Y. X. Yin, Y. G. Guo, L. J. Wan, *Adv. Mater.* **2014**, *26*, 1261–1265; n) X. Yu, A. Manthiram, *Adv. Energy Mater.* **2015**, *5*, 1500350; o) X. Yu, A. Manthiram, *Chem. Mater.* **2016**, *28*, 896–905; p) T. H. Hwang, D. S. Jung, J. S. Kim, B. G. Kim, J. W. Choi, *Nano Lett.* **2013**, *13*, 4532–4538; q) S. Zheng, P. Han, Z. Han, P. Li, H. Zhang, J. Yang, *Adv. Energy Mater.* **2014**, *4*, 1400226.

[6] R. Agrawal, C. Chen, Y. Hao, Y. Song, C. Wang, *Graphene-Based Energy Devices,* Wiley-VCH, Weinheim, **2015**, pp. 171–214.

[7] Y. Hao, X. Li, X. Sun, C. Wang, *Mater. Sci. Eng., B* **2016**, *213*, 83–89.

[8] a) Y. Li, J. Wang, X. Li, D. Geng, M. N. Banis, R. Li, X. Sun, *Electrochem. Commun.* **2012**, *18*, 12–15; b) K. Chang, D. Geng, X. Li, J. Yang, Y. Tang, M. Cai, R. Li, X. Sun, *Adv. Energy Mater.* **2013**, *3*, 839–844; c) X. Wang, X. Li, L. Zhang, Y. Yoon, P. K. Weber, H. Wang, J. Guo, H. Dai, *Science* **2009**, *324*, 768–771; d) J. Xu, M. Wang, N. P. Wickramaratne, M. Jaroniec, S. Dou, L. Dai, *Adv. Mater.* **2015**, *27*, 2042–2048.

[9] G. Zhou, E. Paek, G. S. Hwang, A. Manthiram, *Nat. Commun.* **2015**, *6*, 7760.

[10] Y. Qiu, W. Li, W. Zhao, G. Li, Y. Hou, M. Liu, L. Zhou, F. Ye, H. Li, Z. Wei, *Nano Lett.* **2014**, *14*, 4821–4827.

[11] Z. Wang, Y. Dong, H. Li, Z. Zhao, H. B. Wu, C. Hao, S. Liu, J. Qiu, X. W. D. Lou, *Nat. Commun.* **2014**, *5*, 5002.

[12] R. G. Chaudhuri, S. Paria, *J. Colloid Interface Sci.* **2010**, *343*, 439–446.

[13] a) D. Geng, S. Yang, Y. Zhang, J. Yang, J. Liu, R. Li, T. K. Sham, X. Sun, S. Ye, S. Knights, *Appl. Surf. Sci.* **2011**, *257*, 9193–9198; b) L. Feng, L. Yang, Z. Huang, J. Luo, M. Li, D. Wang, Y. Chen, *Sci. Rep.* **2013**, *3*, 3306; c) L. Qu, Y. Liu, J. B. Baek, L. Dai, *ACS nano* **2010**, *4*, 1321–1326.

[14] a) A. Manthiram, X. Yu, *Small* **2015**, *11*, 2108–2114; b) M. Kohl, F. Borrmann, H. Althues, S. Kaskel, *Adv. Energy Mater.* **2016**, *6*, 1502185.

[15] P. Adelhelm, P. Hartmann, C. L. Bender, M. Busche, C. Eufinger, J. Janek, *Beilstein J. Nanotechnol.* **2015**, *6*, 1016–1055.

[16] W. Shen, C. Wang, Q. Xu, H. Liu, Y. Wang, *Adv. Energy Mater.* **2015**, *5*, 1400982.

Submitted: August 24, 2017
Revised: September 29, 2017
Accepted: October 5, 2017